







## Unidirectional spin Hall magnetoresistance in epitaxial Cr/Fe bilayer from electron-magnon scattering

Thanh Huong Thi Nguyen<sup>1</sup>, Van Quang Nguyen<sup>2</sup>, Seyeop Jeong<sup>2</sup>, Eunkang Park<sup>2</sup>, Heechan Jang<sup>2</sup>, Nyun Jong Lee<sup>2</sup>, Soogil Lee <sup>3</sup>, Byong-Guk Park <sup>3</sup>, Sunglae Cho <sup>2</sup>, Hyun-Woo Lee <sup>4</sup>✉, Jung-Il Hong <sup>1</sup>✉ & Sanghoon Kim <sup>2</sup>✉

Unidirectional Spin Hall magnetoresistance (USMR) is a non-linear phenomenon recently observed in ferromagnet (FM)/nonmagnetic metal (NM) bilayer structures. Two very different mechanisms of USMR have been proposed; one relies on the current-direction-dependence of electron-magnon scattering in a FM layer, and the other on the current-direction-dependence of the spin accumulation at the FM/NM interface. In this study, we investigate the USMR in epitaxial Cr/Fe bilayers finding that the USMR is significantly enhanced when the Fe magnetization is aligned to a particular crystallographic direction where the magnon magnetoresistance (MMR) by the electron-magnon scattering becomes stronger. This highlights the importance of the electron-magnon scattering for the understanding of USMR in Cr/Fe bilayers. Our result also suggests a route to enhance the efficiency of magnon generation in the magnonic devices. Lastly, we discuss the Ising-type spin exchange as a possible origin of the crystallographic direction dependences of the USMR and the MMR.

<sup>1</sup>Department of Emerging Materials Science, Daegu Gyeongbuk Institute of Science & Technology (DGIST), Daegu 42988, Republic of Korea. <sup>2</sup>Department of Physics and EHSRC, University of Ulsan, Ulsan 44610, Republic of Korea. <sup>3</sup>Department of Materials Science and Engineering, Korea Advanced Institute of Science & Technology (KAIST), Daejeon 34141, Republic of Korea. <sup>4</sup>Department of Physics, Pohang University of Science and Technology (POSTECH), Pohang 37673, Republic of Korea. ✉email: [hwl@postech.ac.kr](mailto:hwl@postech.ac.kr); [jihong@dgist.ac.kr](mailto:jihong@dgist.ac.kr); [sanghoon.kim@ulsan.ac.kr](mailto:sanghoon.kim@ulsan.ac.kr)

Spin Hall effect (SHE) is an essential mechanism through which pure spin current can be generated in various non-magnetic matters (NM), such as Pt, W, Ta, topological insulators, and semimetals. SHE effectively produces spin accumulation at the edges in the spin Hall materials. When they are in contact with a ferromagnetic (FM) layer forming bilayers, SHE can give rise to technologically useful phenomena, e.g., magnetization switching<sup>1,2</sup>, magnetic domain wall motion<sup>3,4</sup>, and magnetization oscillation<sup>5,6</sup> due to the spin torque actions of polarized spin current. Other than magnetization manipulation, novel transport properties have also been reported. For instance, the resistance of the bilayer varies depending on whether the spin polarization ( $\sigma$ ) of the SHE-induced spin current is collinear or perpendicular to the magnetization ( $M$ ) of FM. Such directional dependence in the linear response regime is called spin Hall magnetoresistance (SMR)<sup>7,8</sup>. Another SHE-related MR appears in the nonlinear regime as well; when  $\sigma$  and  $M$  are collinear, the resistance for parallel  $\sigma$  and  $M$  differs from that for antiparallel  $\sigma$  and  $M$ . Since  $\sigma$  reverses its sign as the current density ( $J$ ) reverses its sign, the resistance for one particular  $J$  direction can be larger than that for the opposite  $J$  direction. Such dependence in the nonlinear regime is called unidirectional spin Hall magnetoresistance (USMR)<sup>9–12</sup>. Therefore, the magnitude of USMR should depend on both  $J$  and relative directions, parallel or antiparallel, between  $\sigma$  and  $M$ . In other words, this spin configuration results in an asymmetry in longitudinal resistance of the systems.

Two possible mechanisms have been proposed for a better understanding of USMR. The very first experimental report on the USMR proposed the spin accumulation by SHE at the NM/FM interface as the origin of USMR; the variation of spin accumulation at the interface between NM and FM modulates the interface scattering potential and hence the interfacial resistance. This is analogous to the interfacial contribution of giant magnetoresistance (GMR)<sup>9,13</sup>. Later experimental observations on topological insulators/FM bilayers proposed a qualitatively different mechanism<sup>11,14</sup>, which has no analogy to the interfacial contribution of GMR. This mechanism attributes the USMR to the electron–magnon scattering; the spin current may create or annihilate magnons depending on the  $\sigma$  direction of spin current and the resulting change in the magnon number modulates the electron–magnon scattering contribution to the resistance. USMR has been observed in various bilayer structures with different underlying mechanisms. The modification of the interfacial resistance (or the spin-dependent scattering) has been taken into account to explain the observed USMR in heavy metal (HM)/FM metal bilayers, such as Pt/Co, Ta/Co<sup>9</sup>. Exploiting this mechanism, a thin Cu (or Ag) interlayer is inserted into the HM/FM interface in an attempt to enhance USMR further<sup>15</sup>. Meanwhile, another mechanism based on the electron–magnon scattering is invoked to interpret USMR observed in topological insulators (TIs)<sup>11,14,16</sup>. Later experiments<sup>12,17,18</sup> argued that the electron–magnon scattering mechanism of the USMR may contribute to the USMR in conventional NM/FM metallic bilayers as well. However, the nature of the electron–magnon scattering mechanism of the USMR is not yet clearly resolved. Issues include the applicability of the mechanism to NM/FM insulator bilayers<sup>19</sup>, energy scales of relevant magnons (dipolar magnons of  $\sim 1 \mu\text{eV}$ <sup>18</sup> vs. relatively high-energy magnons of  $\sim 1 \text{meV}$ <sup>12</sup>), and the scaling of the mechanism with respect to the spin Hall angle (linear<sup>12</sup> and cubic<sup>18</sup>). Above all, however, more persuasive experimental evidence of the electron–magnon scattering mechanism of the USMR itself are still desired.

In the present study, we investigate the USMR in epitaxial Cr/Fe bilayers. The epitaxy of systems allows one to examine the crystallographic dependence of USMR, which has not been achieved in the previous experimental studies. We find that the USMR in our

metallic bilayers depends strongly on the crystallographic orientation along which electrical current flows. Such crystallographic dependence of the USMR differs qualitatively from that of the SMR but agrees with that of the magnon magnetoresistance (MMR), implying that the USMR in the Cr/Fe film arises mainly by the electron–magnon scattering mechanism. As a possible origin of the crystallographic directional dependence in the MMR and the USMR, we consider an Ising-type exchange interaction. We demonstrate that if the exchange interaction is stronger for one particular component of magnetization direction (thus Ising-character exchange), magnon generation becomes more efficient when the magnetization is aligned along the stronger exchange direction. Our study provides a new route to enhance the efficiency of magnon generation in magnonic devices.

## Results

**Crystalline structures and magnetic properties of the epitaxially grown Cr/Fe bilayers.** Cr/Fe thin films were grown on (110) and (100)-oriented MgO substrates using molecular beam epitaxy (MBE) (see the details in the “Method” section). The crystalline quality of the films was then examined via high-resolution transmission electron microscopy (HRTEM). Cross-sectional HRTEM images of the Cr/Fe films on MgO (110) and (100) substrates are shown in Fig. 1a–c, respectively. The images clearly reveal that the growth mode for Cr/Fe films on both MgO (110) and MgO (100) substrates was the Frank-van der Merwe type (layer growth mode) forming atomically flat interfaces. The analyses of HRTEM results also indicate the epitaxial growth of Cr/Fe (211) on MgO (110) (Fig. 1a, b) and of Cr/Fe (100) on MgO (100) (Fig. 1c). The crystallographic orientations in the films and the substrates are determined: Cr/Fe (211) [0–11]//MgO (110) [001], Cr/Fe (211) [–111]//MgO (110) [–110], and Cr/Fe (100) [110]//MgO (001) [100]. Analogous growth directions of the Cr/Fe have previously been observed in literature<sup>20–22</sup>. The lattice strain in the Cr/Fe films was estimated from the HRTEM images; the tensile strain of +3.43% was induced along [0–11] direction (Fig. 1d), due to the lattice mismatch of –4.5%. Meanwhile, with a remarkably large lattice mismatch of –17.30% along [–111] direction, the epitaxial relationship could not be established at the interface in this direction. However, the lattice was examined to be slightly compressed by –0.80% (see in Fig. 1d). The Fourier filtered image (inset in Fig. 1b) clearly showed that dislocations were introduced during the deposition at the interface between the MgO substrate and the subsequent Cr layer to relax the large lattice mismatch. On the other hand, the TEM analyses for the Cr/Fe (100) film, exhibiting a lattice mismatch of –4.5% with the MgO substrate, showed that  $d$ -spacing in the [110] direction was slightly elongated by 0.98% (Fig. 1e).

We next investigate the magnetic properties of the Cr/Fe films. Figure 1f, g shows magnetization curves for the Cr/Fe (211) and the Cr/Fe (100) films, respectively. From the ratio of remanent magnetization to the saturation magnetization ( $M_r/M_s$ ), two distinct behaviors of the two sets of samples could be readily recognized. As clearly seen in Fig. 1f, the Cr/Fe (211) film exhibits a twofold symmetry; a hard axis is parallel to [–102] direction and an easy axis is parallel to [2–51] direction. This uniaxial-like anisotropy can be attributed to the lattice strain in the film, which is an important character of the Cr/Fe (211) film in the present study. Meanwhile, a fourfold symmetry is observed in the Cr/Fe (100) film with a hard axis along [110] and an easy axis along [100], reflecting the typical magnetic anisotropy of bcc-Fe crystal.

**USMR of the Cr/Fe bilayers.** Five devices with respective current flow directions were prepared in order to investigate the crystallographic dependence of USMR, as schematically shown in

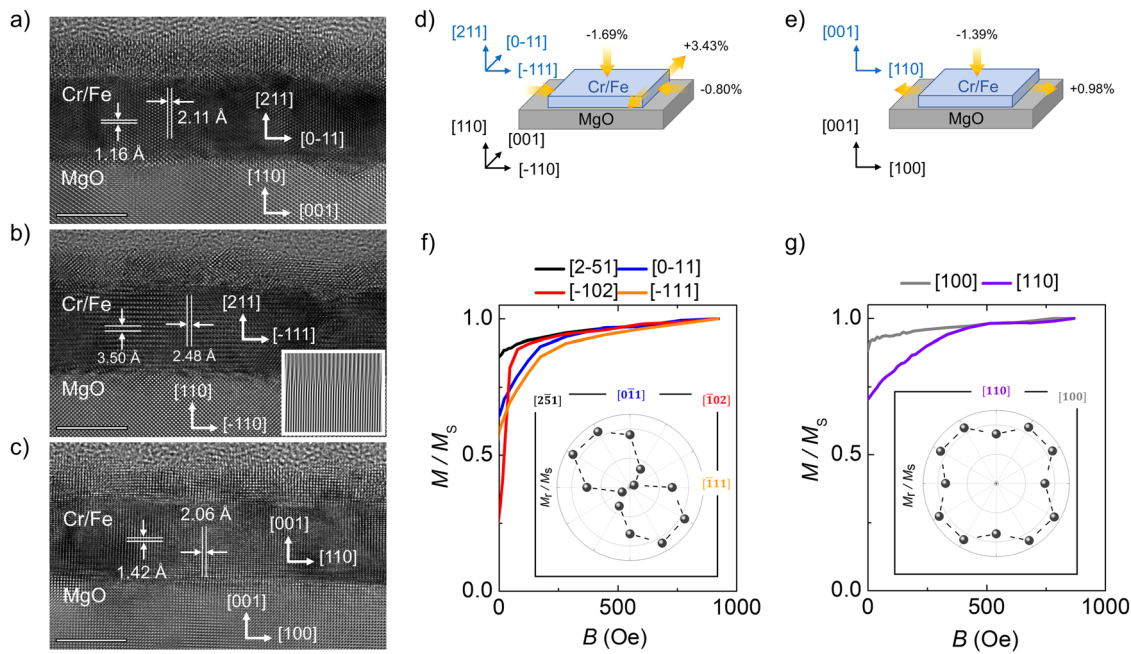


**Fig. 1 Crystalline structures and magnetic properties of the epitaxially grown Cr/Fe bilayers.** **a–c** Cross-sectional high-resolution transmission electron microscopy (HRTEM) images of Cr/Fe bilayer films on MgO substrates with MgO (110) [–111] zone axis (**a**), MgO (110) [0–11] zone axis (**b**), and MgO (100) [100] zone axis (**c**). Inset in (**b**) is a Fourier filter image of the interface between the MgO substrate and the subsequent Cr layer. Scale bar: 5 nm. **d**, **e** 3D schematics of Cr/Fe bilayer films on MgO (110) substrate (**d**) and MgO (100) substrate (**e**) with an explanation of crystallographic orientation relationship between films and substrates. Induced strains are also indicated by yellow arrows. **f**, **g** Normalized magnetization curves ( $M/M_s$ ) of Cr/Fe (211) film (**f**) and Cr/Fe (100) film (**g**) along specific directions. The insets show polar plots of the ratio of remanent magnetization ( $M_r$ ) to the saturation magnetization ( $M_s$ ) obtained from in-plane hysteresis loops of corresponding films.

Fig. 2a, b. Specific crystallography directions are indicated by the arrows. Five devices are labeled as  $I102$ ,  $I111$ ,  $I011$ ,  $I110$ ,  $I100$ , in correspondence to the crystallographic directions, [–102], [–111], [0–11], [110], and [100] of the current flow, respectively. Figure 2c shows the USMR measurement results at various current flow directions using a second harmonic measurement at room temperature. The longitudinal resistance ( $R_{2\omega}$ ) was measured when an external magnetic field ( $B$ ) was swept along  $y$ -axis (see an optical microscope image in Fig. 2d). It is reported that the  $R_{2\omega}$  changes sign upon the reversal of the magnetization direction<sup>9</sup>. We observed that USMR of Cr-based bilayer films show the same sign as that of Ta-based sample but opposite to that of Pt-based sample (see the Supplementary Note 1), in consistency with the previous reports on the sign of effective spin Hall angle of Cr-based systems<sup>23,24</sup>.

Angular dependence of  $R_{xx}$  was further investigated as shown in Fig. 2e, f. The first harmonic component  $R_\omega$  and the second harmonic component  $R_{2\omega}$  of  $R_{xx}$  were simultaneously measured as a function of azimuthal angle  $\varphi$  between the applied current  $\mathbf{J}$  and the magnetic field  $B$ . While  $R_\omega$  shows expected AMR behavior ( $\cos 2\varphi$  dependence) for a FM at saturated magnetization state, the  $R_{2\omega}$  signal is proportional to  $-\sin\varphi$ , showing an identical symmetry to the field sweep measurement of USMR.

Thermoelectric effects, such as the anomalous Nernst effect and the spin Seebeck effect may generate similar  $\sin\varphi$ -type contribution to the longitudinal voltage due to heat gradient ( $M \perp VT \perp J_e$ ). Hence,  $R_{2\omega} = R_{2\omega}^{\text{USMR}} + R_{2\omega}^{\text{VT}}$ , where  $R_{2\omega}$ ,  $R_{2\omega}^{\text{USMR}}$ ,  $R_{2\omega}^{\text{VT}}$  is total second harmonic resistance, intrinsic USMR and resistance emerged from thermoelectric voltages, respectively. To subtract the  $R_{2\omega}^{\text{VT}}$ , we quantitatively evaluate the thermoelectric voltages by conducting the angular dependence measurement of the second harmonic planar Hall effect. Details of this evaluation procedure can be found elsewhere<sup>25</sup>. We found that the  $R_{2\omega}^{\text{VT}}$  is nearly negligible in Cr/Fe

(211) samples while it is  $\sim 0.74$  m $\Omega$  in  $I110$  sample and  $\sim 0.61$  m $\Omega$  in  $I100$  sample, which is  $\sim 21.1\%$  and  $\sim 18.8\%$  of the total  $R_{2\omega}$ , respectively.

To compare the  $R_{2\omega}^{\text{USMR}}$  values between samples, we measured USMR with respect to current density ( $J$ ) for all samples. The plots of  $R_{2\omega}^{\text{USMR}} (= R_{2\omega} - R_{2\omega}^{\text{VT}})$  vs.  $J$  are presented in Fig. 3a and the normalized  $R_{2\omega}^{\text{USMR}} (= R_{2\omega}^{\text{USMR}}/J)$  with respect to the current density are summarized in Fig. 3b (see Supplementary Note 2 for USMR results in larger  $J$  range). As expected, the observed USMR is linearly proportional to  $J$  for all samples. Here, we note that USMR as a function of  $J$  shows strong crystallographic dependence. It is notable that the  $R_{2\omega}^{\text{USMR}}$  of  $I102$  shows the maximum value (about 3 times larger than others) among the samples while  $R_{2\omega}^{\text{USMR}}$ 's of others are comparable with each other; the normalized  $R_{2\omega}^{\text{USMR}}$  of  $I110$  on (100) film is slightly greater than that of the  $I011$  on (211) film.

**Spin Hall magnetoresistance of the Cr/Fe bilayers.** In order to examine the origin of the crystallographic dependence of the normalized  $R_{2\omega}^{\text{USMR}}$ , we conducted another spin-related transport measurement, that is, SMR which also occurs in an NM/FM bilayer system via SHE. Generally, the SMR refers to variation in the total resistance of the NM/FM bilayer system, in which spin current is generated within the NM layer, thus resulting in a spin accumulation at the interface between NM and FM. Depending upon the direction of the spin polarization at the interface with respect to the  $M$  of the FM layer (either collinear or perpendicular), the back-flow of spin current is added to (subtracted from) the total charge current going through the bilayer, thus leading to an increase (decrease) of the total resistance<sup>7,8,10</sup>.

Figure 4b, c shows SMR results for all samples. The longitudinal resistance,  $R_{xx}(B_z)$  and  $R_{xx}(B_y)$ , was measured as

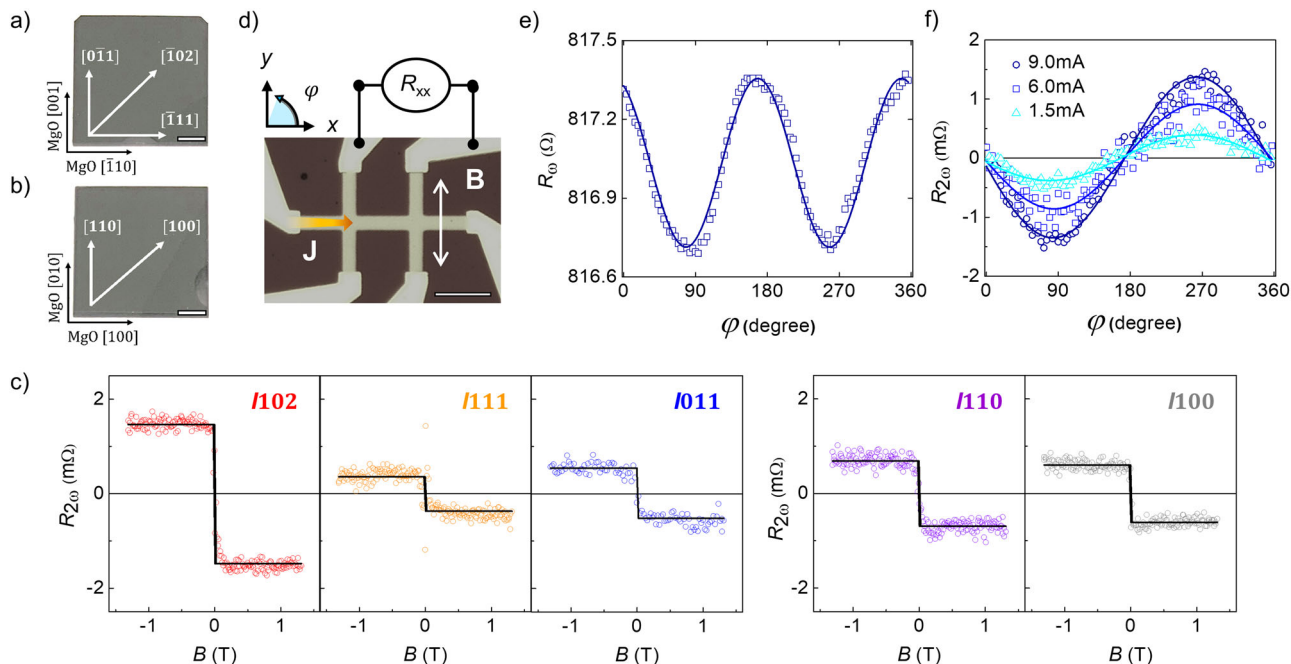


**Fig. 2 Unidirectional spin Hall magnetoresistance of the Cr/Fe bilayers.** **a, b** Images of Cr/Fe films on MgO (110) substrate (**a**) and MgO (100) substrate (**b**). The arrows indicate five specific crystallographic directions. Scale bar: 2 mm. **c** Unidirectional spin Hall magnetoresistance (USMR) measurement results measured by second harmonic voltage via field dependence configuration for /102 (red), /111 (orange), /011 (blue), /110 (purple), and /100 (gray). Solid lines are fitted to the data using the step function. **d** An optical microscope image of an H-shape Hall bar pattern after the patterning process. Scale bar: 50  $\mu\text{m}$ . Schematic of USMR measurement configuration defines applied current  $J$  (yellow arrow), the sweeping direction of external magnetic field  $B$  (white double arrow) in field dependence measurement, and azimuthal angle  $\varphi$  between  $J$  and  $B$  in angular dependence measurement. **e, f** The first harmonic component  $R_{\omega}$  (**e**) and the second harmonic component  $R_{2\omega}$  (**f**) of angular dependence USMR measurement results for /102. Solid lines are fitted to the data using  $\cos 2\varphi$  function (**e**) and  $-\sin\varphi$  function (**f**). The error bars are obtained as the mean of repeated measurements and are smaller than the size of the data markers.

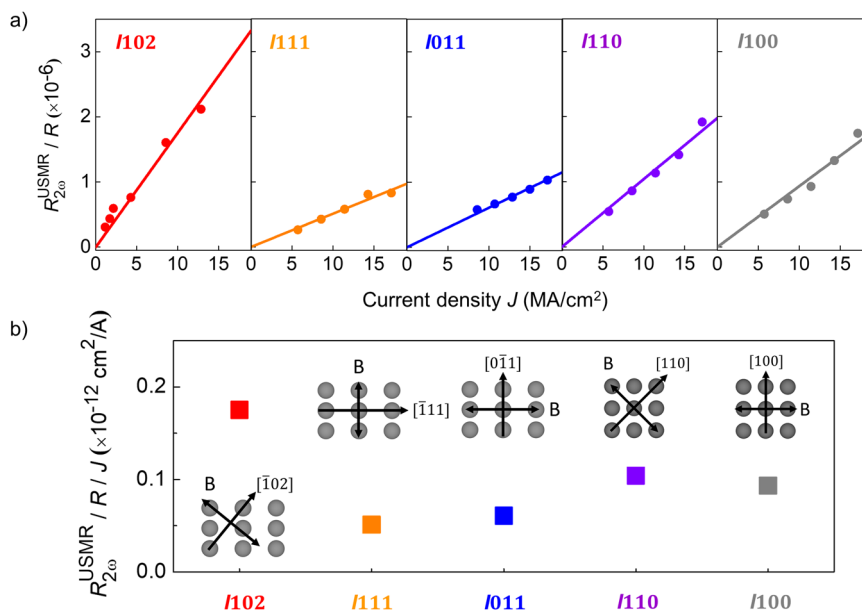


**Fig. 3 Normalized unidirectional spin Hall magnetoresistance of the Cr/Fe bilayers.** **a** Variation of unidirectional spin Hall magnetoresistance (USMR) value ( $R_{2\omega}^{\text{USMR}}/R$ ) as a function of current density ( $J$ ) for /102 (red), /111 (orange), /011 (blue), /110 (purple), and /100 (gray). Solid lines are fitted to the data using a linear function. **b** Comparison of normalized USMR ( $R_{2\omega}^{\text{USMR}}/J$ ) between devices with the various crystallographic directions where current flows. The insets schematically show atomic arrangements (gray solid circles) with arrows indicating the current flowing direction and the external magnetic field ( $B$ ) direction in each device. The error bars correspond to standard deviation and are smaller than the size of the data markers.

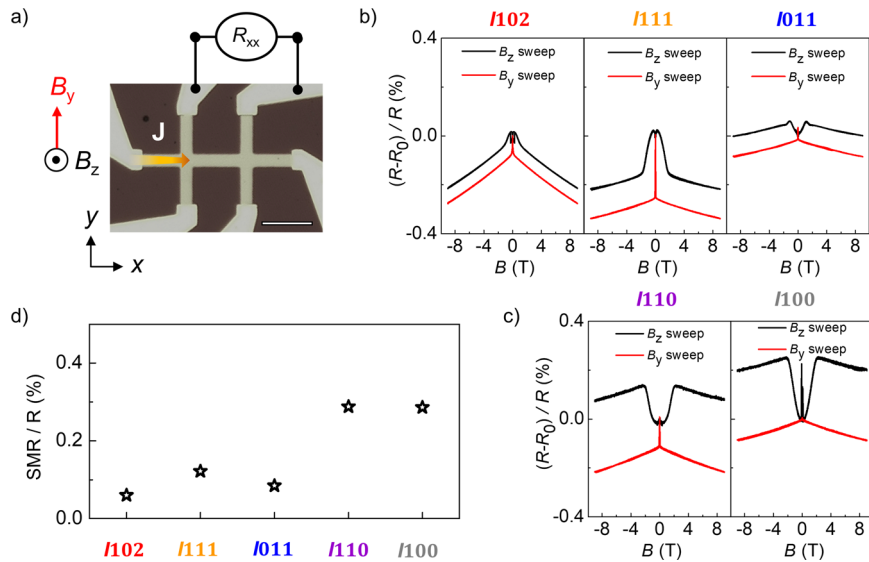


**Fig. 4** Spin Hall magnetoresistance of the Cr/Fe bilayers. **a** Schematic of spin Hall magnetoresistance (SMR) measurement configuration. The longitudinal resistances ( $R_{xx}$ ) were measured as the current ( $J$ ) is applied along  $x$ -axis and the magnetic field was swept along  $z$ -axis ( $B_z$ ) and  $y$ -axis ( $B_y$ ). **b, c** Longitudinal magnetoresistance ( $(R_{xx} - R_0)/R_{xx}$ , where  $R_0$  is  $R_{xx}$  at zero field) plotted against external magnetic field along  $z$ -axis (black) and  $y$ -axis (red) for I102, I111, I011 devices on Cr/Fe (211) (**b**) and I110, I100 devices on Cr/Fe (100) (**c**). **d** Comparison of normalized SMR between samples, where  $SMR = R_{xx}(B_z) - R_{xx}(B_y)$  in saturated magnetization field range. The error bars correspond to standard deviation and are smaller than the size of the data markers.

the magnetic field was swept along  $z$ -axis ( $B_z$ ) and  $y$ -axis ( $B_y$ ), respectively (Fig. 4a). SMR is deduced by taking the difference of two resistances under saturated magnetization field range:  $SMR = R_{xx}(B_z) - R_{xx}(B_y)$ , as shown in Fig. 4d. We find that the SMR data of the devices do not reproduce the trend of the normalized  $R_{2\omega}^{USMR}$ . In particular, the I102 sample exhibits the smallest SMR, and the devices on the MgO (100) substrate show almost three times greater SMR than those on the MgO (110) substrate. According to the previous literature<sup>7,26</sup>, there are four crucial parameters for SMR, i.e., spin Hall angle of the NM ( $\theta_{SH}$ ), the spin diffusion length of the NM ( $\lambda_{NM}$ ), spin mixing conductance at the interface ( $G_r$ ), and the spin polarization of the FM ( $P$ ). The SMR results show that none of those parameters can explain the trend of USMR measured in this study, suggesting that other origin should be considered.

**Magnon magnetoresistance of the Cr/Fe bilayers.** As mentioned in the introduction, there are two possible origins of USMR. We now focus on the electron–magnon scattering mechanism of USMR. In order to examine the relevance of the electron–magnon scattering mechanism, another MR measurement was then conducted, as was first proposed by Raquet et al.<sup>27</sup>. Their work has built a theoretical model to explain experimental observations on electrical transport properties of  $3d$  metals (Fe, Co, and Ni) under high magnetic field regime over 9 T. Figure 5a, b shows the MR of our samples with in-plane field sweep. The field sweep axis is perpendicular to the current direction. As revealed in B. Raquet’s study, the resistivity is negatively and linearly proportional to the magnetic field in the high magnetic field range over 9 T. This phenomenon is referred as so-called high-energy MMR, attributed to the electron–magnon scattering. In our study, we also find the high-energy MMR in the Cr/Fe samples. Figure 5c, d shows the slope of the resistance ( $dR/dB$ ) in a range of 7–9 T, which is related to the number of electron–magnon scattering events. The slope can be described as<sup>27</sup>

$$\frac{\partial \Delta \rho_{\text{mag}}(T, B)}{\partial B} \propto T(1 + 2d_1 T^2)(\ln T), \quad (1)$$

where  $d_1$  is a parameter related to decrease in the exchange stiffness  $A$ . The  $A$  is known to be a  $T$ -dependent parameter described as<sup>27</sup>

$$A \propto A_0(1 - d_1 T^2). \quad (2)$$

From Eq. (2), one should expect that larger  $d_1$  results in smaller  $A$ . In other words, magnons are generated more efficiently along the direction where exchange stiffness is small and vice versa. This has explicitly explained the difference in slopes of the resistance ( $\sigma$ ) in the range of 7–9 T. Note that the MMRs with various current directions exhibit the same crystallographic direction dependence as what the USMR does. This indicates the importance of the electron–magnon scattering mechanism for the USMR in Cr/Fe bilayers. The absolute values of both the MMR and the USMR are different from each other because they are induced by thermally induced and current-induced magnons, respectively. Further details on this point are discussed in Supplementary Note 3. In this study, we focus on the similar trends between the two MRs to understand the magnon contribution to the USMR, as discussed in the next section.

## Discussion

The same crystallographic dependence of the MMR and the USMR implies that they may share a common origin (Fig. 5e). Raquet et al.<sup>27</sup> attributed the MMR to the electron–magnon scattering with rather high-energy magnons. For conventional  $3d$  FMs Fe, Co, and Ni, they estimated that magnons with energies up to 150 meV are involved in the electron–magnon scattering at room temperature. Although 150 meV is higher than the room temperature scale  $\sim 25$  meV and the population of such high energy magnons are rather suppressed, they may be still important sources of resistivity since they have large momenta and thus cause large-angle deflection of electrons. Energy scale information can be obtained also from our USMR result. We find that the USMR remains almost constant up to the highest field of 9 T used in our experiment (Fig. 5f), meaning that the magnons responsible for the USMR in the Cr/Fe bilayer are not suppressed even in the high magnetic field range, as reported with a Pt/Py bilayer

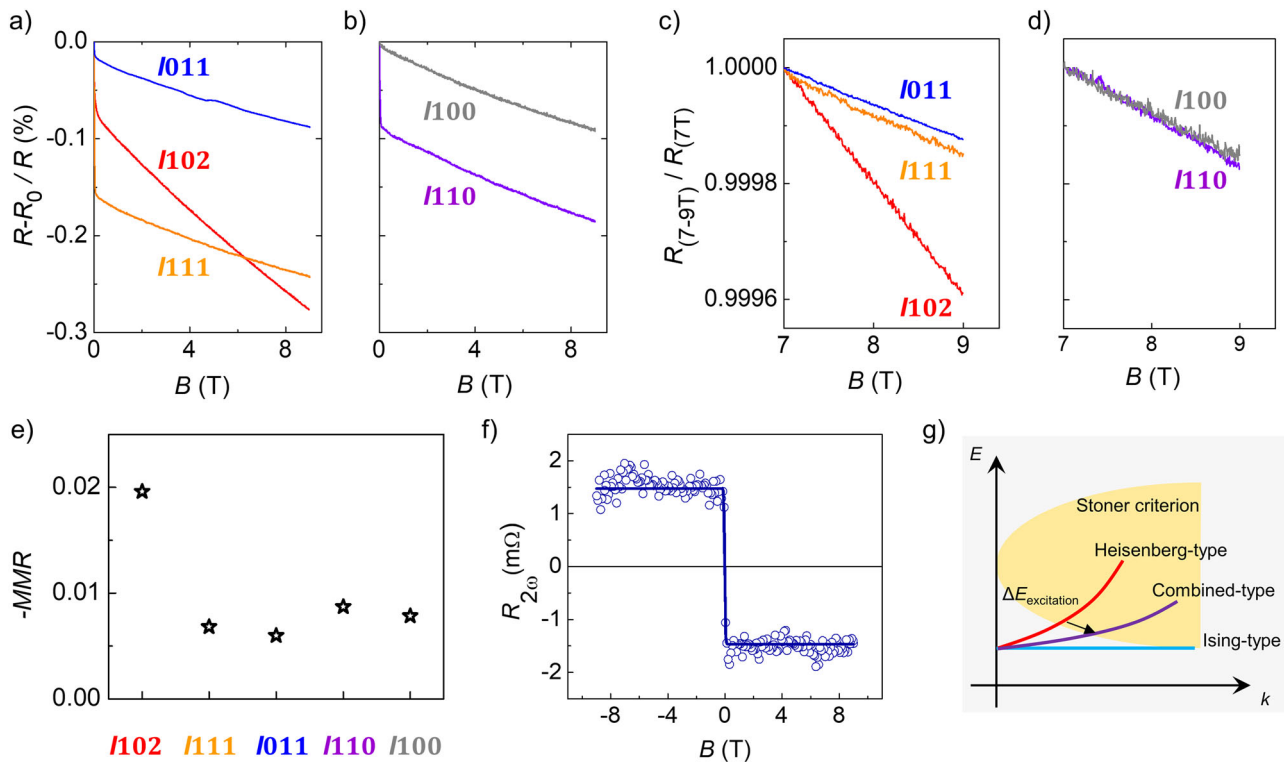


**Fig. 5** Magnon magnetoresistance of the Cr/Fe bilayers. **a, b** Longitudinal magnetoresistance  $((R - R_0)/R)$  plotted against external magnetic field  $B$  along  $y$ -axis for devices on Cr/Fe (211) (**a**) and Cr/Fe (100) (**b**). **c, d** High field regime (7–9 T) of longitudinal magnetoresistance. The resistance value is normalized by its value at 7 T ( $R_{7-9T}/R_{7T}$ ). **e** Comparison between samples of magnon magnetoresistance ( $-MMR$ ) values which are extracted slopes of longitudinal magnetoresistance in high magnetic field range. **f** Unidirectional spin Hall magnetoresistance (USMR) result measured up to 9 T for I102 device with  $J = 1.29 \times 10^7 \text{ A cm}^{-2}$ . A solid line is fitted to the data using the step function. **g** Schematic illustrates Stoner criterion (yellow region) and the magnon dispersion relation of a ferromagnetic system with Heisenberg exchange interaction (red line), Ising exchange interaction (blue line), and a combination of the two exchange types (purple line). The arrow indicates that the energy required for magnon excitation via spin-flip process in the combining case is lower than that in the Heisenberg-type case.

systems<sup>12</sup>. Here, the lower bound of the magnon energy scale could be estimated using  $g\mu_B B$  and  $g = 2$  to be approximately 0.9 meV. Therefore, both USMR and the MMR indicate the high-energy nature of magnons in the epitaxial Cr/Fe bilayer. The high-energy magnon is known to be important in spin-flip process, known as Stoner excitation<sup>12,28</sup>. In other words, when spin current is injected from NM to FM layers, conduction electrons in the FM layer jump from majority to minority band, resulting in the generation of high energy magnons, thereby enhancing the electron–magnon scattering and resulting in the USMR<sup>12</sup>. On the other hand, a recent experiment<sup>18</sup> found the correlation between the USMR and the dipolar magnon density and attributed the USMR to the electron–magnon scattering with dipolar magnons of 10–20 GHz frequency scale. Thus although both our result and I.V. Borisenko’s result<sup>18</sup> imply the importance of the electron–magnon scattering, the energy scale estimation is different. Further study is needed to clarify this issue.

Here, we note that the USMR and MMR in the device I102 is significantly higher in magnitude as compared to those of other samples. In order to understand such high values along a specific crystallographic direction, we first note that the MMR is inversely proportional to  $A$ <sup>27</sup>. This naturally leads to the speculation that the crystallographic direction dependence may arise from the directional dependence of the exchange interaction. To examine this possibility, we consider the magnon energy dependence on the exchange interaction. The magnon dispersion can be considered with the Landau–Lifshitz equation of motion:  $\frac{\partial \hat{m}}{\partial t} = -\gamma \hat{m} \times \vec{H}_{\text{eff}}$ . In conventional FMs with the isotropic

Heisenberg-type exchange,  $\vec{H}_{\text{eff}} = K_z m_z \hat{z} + A \nabla^2 \hat{m}$  describes a system in a presence of magnetic anisotropy and an exchange interaction. The magnon angular frequency (magnon dispersion) is then given by  $\omega = \gamma(K_z + Ak^2)$ , which shows quadratic dependence on the wave vector  $k$ . However, the stand-alone Heisenberg-type exchange cannot explain such crystallographic dependence of the observed USMR and MMR. Remarkably, the independent studies on 2D Heisenberg systems reveal that Ising-type exchange interaction also exists in the system hosting a uniaxial magnetic anisotropy<sup>29,30</sup>. Motivated by these studies and also considering that the Cr/Fe (211) film clearly exhibits the uniaxial magnetic anisotropy (see Fig. 1f), we examine the extreme case; the second term is now given by  $A_z \nabla^2 m_z \hat{z}$ , where  $z$  is an easy axis. This means that there is no contribution from exchange interaction out of the easy axis. The participation of Ising exchange interaction leads to the dispersion  $\omega = \gamma K_z$ , which is constant with magnon wave vector  $k$  as shown in Fig. 5g. The detailed derivation can be found in Supplementary Note 4. In more realistic situations where both the Heisenberg-type exchange interaction and Ising-type exchange interaction co-exist along the magnetic easy axis, the presence of the Ising-type character can result in a lower barrier to reach the Stoner criterion for the more spin-flip-induced (high energy) magnon excitation, as described in Fig. 5g. Although further study is indeed required to manifest those mentioned above, our results clearly show that the spin-flip process and the resultant high-energy magnon generation strongly depend on the crystallographic direction.

In conclusion, the USMR of the epitaxial Cr/Fe bilayers shows a clear dependence on crystallographic orientation. The bcc Cr/Fe structure can be epitaxially grown with two different orientations, and the five crystallographic orientations are selected to measure the USMR. Our systematic approach reveals the importance of the electron–magnon scattering mechanism, which associates the USMR with high-energy magnon contributions to the electron–magnon scattering. It implies that high-energy magnon generated via quantum spin–flip process plays a significant role in spin-dependent transport of metallic bilayers. We also find that the Ising-type character of the magnetic thin film can induce magnon generation efficiently. Hence, our findings can be broadly utilized for the development of various magnonic devices.

## Methods

**Film growth.** The Cr (5 nm)/Fe (2 nm)/Mg (1 nm)/MgO<sub>x</sub> (2 nm) were grown onto the MgO (110) and MgO (100) substrates via MBE at an ultrahigh vacuum of 10<sup>−9</sup> Torr. The growth temperature was 150 °C. Afterward, a capping layer Ta (4 nm) was deposited by RF sputtering and then naturally oxidized at ambient conditions.

**TEM.** The TEM specimens were prepared using the dual-beam focused ion beam (Hitachi NB 5000). HR-TEM images were captured using a Hitachi HF-3300 microscope with a field emission gun operated at 300 kV. Sample preparation and TEM measurement were performed at the DGIST Center for Core Research Facilities (CCRF), Korea.

**Device fabrication.** The samples were patterned into typical Hall bars via standard photolithography and followed by Ar ion milling process. The current linewidth *w* is 10 μm and the distance between two Hall branches *l* is 60 μm. Finally, the six Ru contact pads were deposited by sequentially means of photolithography, RF sputtering and lift-off process.

**MR measurements.** The USMR experiment was carried out by applying an AC current with a frequency of 137 Hz along *x*-axis. The longitudinal magnetoresistance measured in SMR and MMR measurement was carried out by applying DC current along *x*-axis. All measurements were conducted at room temperature.

## Data availability

The data collected during this study are available from the corresponding author upon reasonable request.

Received: 14 May 2021; Accepted: 25 October 2021;

Published online: 18 November 2021

## References

- Fan, Y. et al. Magnetization switching through giant spin-orbit torque in a magnetically doped topological insulator heterostructure. *Nat. Mater.* **13**, 699–704 (2014).
- Garello, K. et al. Ultrafast magnetization switching by spin-orbit torques. *Appl. Phys. Lett.* **105**, 212402 (2014).
- Haazen, P. P. et al. Domain wall depinning governed by the spin Hall effect. *Nat. Mater.* **12**, 299–303 (2013).
- Emori, S., Bauer, U., Ahn, S. M., Martinez, E. & Beach, G. S. Current-driven dynamics of chiral ferromagnetic domain walls. *Nat. Mater.* **12**, 611–616 (2013).
- Liu, L., Moriyama, T., Ralph, D. C. & Buhrman, R. A. Spin-torque ferromagnetic resonance induced by the spin Hall effect. *Phys. Rev. Lett.* **106**, 036601 (2011).
- Liu, L., Pai, C. F., Ralph, D. C. & Buhrman, R. A. Magnetic oscillations driven by the spin Hall effect in 3-terminal magnetic tunnel junction devices. *Phys. Rev. Lett.* **109**, 186602 (2012).
- Althammer, M. et al. Quantitative study of the spin Hall magnetoresistance in ferromagnetic insulator/normal metal hybrids. *Phys. Rev. B* **87**, 224401 (2013).
- Nakayama, H. et al. Spin Hall magnetoresistance induced by a nonequilibrium proximity effect. *Phys. Rev. Lett.* **110**, 206601 (2013).
- Avci, C. O. et al. Unidirectional spin Hall magnetoresistance in ferromagnet/normal metal bilayers. *Nat. Phys.* **11**, 570–575 (2015).
- Avci, C. O. et al. Magnetoresistance of heavy and light metal/ferromagnet bilayers. *Appl. Phys. Lett.* **107**, 192405 (2015).

- Yasuda, K. et al. Large unidirectional magnetoresistance in a magnetic topological insulator. *Phys. Rev. Lett.* **117**, 127202 (2016).
- Kim, K.-J. et al. Possible contribution of high-energy magnons to unidirectional magnetoresistance in metallic bilayers. *Appl. Phys. Express* **12**, 063001 (2019).
- Zhang, S. S. L. & Vignale, G. Theory of unidirectional spin Hall magnetoresistance in heavy-metal/ferromagnetic-metal bilayers. *Phys. Rev. B* **94**, 140411(R) (2016).
- Duy Khang, N. H. & Hai, P. N. Giant unidirectional spin Hall magnetoresistance in topological insulator–ferromagnetic semiconductor heterostructures. *J. Appl. Phys.* **126**, 233903 (2019).
- Hasegawa, K., Koyama, T. & Chiba, D. Enhanced unidirectional spin Hall magnetoresistance in a Pt/Co system with a Cu interlayer. *Phys. Rev. B* **103**, L020411 (2021).
- Fan, Y. et al. Unidirectional magneto-resistance in modulation-doped magnetic topological insulators. *Nano Lett.* **19**, 692–698 (2019).
- Avci, C. O., Mendil, J., Beach, G. S. D. & Gambardella, P. Origins of the unidirectional spin hall magnetoresistance in metallic bilayers. *Phys. Rev. Lett.* **121**, 087207 (2018).
- Borisenko, I. V., Demidov, V. E., Urazhdin, S., Rinkevich, A. B. & Demokritov, S. O. Relation between unidirectional spin Hall magnetoresistance and spin current-driven magnon generation. *Appl. Phys. Lett.* **113**, 062403 (2018).
- Sterk, W. P., Peerlings, D. & Duine, R. A. Magnon contribution to unidirectional spin Hall magnetoresistance in ferromagnetic-insulator/heavy-metal bilayers. *Phys. Rev. B* **99**, 064438 (2019).
- Fullerton, E. E., Conover, M. J., Mattson, J. E., Sowers, C. H. & Bader, S. D. Oscillatory interlayer coupling and giant magnetoresistance in epitaxial Fe/Cr(211) and (100) superlattices. *Phys. Rev. B Condens. Matter* **48**, 15755–15763 (1993).
- Jiang, J. S. et al. Exchange-bias effect in Fe/Cr(211) double superlattice structures. *Phys. Rev. B* **61**, 9653 (2000).
- Serizawa, K. et al. Influence of crystal orientation on the magnetostriction behavior of Fe films formed on MgO single-crystal substrates. *J. Magn. Magn. Mater.* **477**, 420–426 (2019).
- Wen, Z., Kim, J., Sukegawa, H., Hayashi, M. & Mitani, S. Spin-orbit torque in Cr/CoFeAl/MgO and Ru/CoFeAl/MgO epitaxial magnetic heterostructures. *AIP Adv.* **6**, 056307 (2016).
- Chuang, T. C., Pai, C. F. & Huang, S. Y. Cr-induced perpendicular magnetic anisotropy and field-free spin-orbit-torque switching. *Phys. Rev. Appl.* **11**, 061005 (2019).
- Avci, C. O. et al. Interplay of spin-orbit torque and thermoelectric effects in ferromagnet/normal-metal bilayers. *Phys. Rev. B* **90**, 224427 (2014).
- Kim, J., Sheng, P., Takahashi, S., Mitani, S. & Hayashi, M. Spin Hall magnetoresistance in metallic bilayers. *Phys. Rev. Lett.* **116**, 097201 (2016). doi:10.1103/PhysRevLett.116.097201
- Raquet, B., Viret, M., Sondergard, E., Cespedes, O. & Mamy, R. Electron-magnon scattering and magnetic resistivity in 3d ferromagnets. *Phys. Rev. B* **66**, 024433 (2002).
- Cornelissen, L. J., Liu, J., Duine, R. A., Youssef, J. B. & van Wees, B. J. Long-distance transport of magnon spin information in a magnetic insulator at room temperature. *Nat. Phys.* **11**, 1022–1026 (2015).
- Elmers, H. J., Hauschild, J., Liu, G. H. & Gradmann, U. Critical phenomena in the two-dimensional XY magnet Fe(100) on W(100). *J. Appl. Phys.* **79**, 4984 (1996).
- Liu, C. & Bader, S. D. Magnetic properties of ultra thin epitaxial films of iron. *J. Magn. Magn. Mater.* **93**, 307–314 (1991).

## Acknowledgements

This work was supported by the National Research Foundation of Korea (NRF) grants funded by the Korean government (MSIT) (NRF- 2019R1C1C1010345, 2020R1A2C2005932, 2018R1A5A6075964 and 2020R1A2C2013484, 2020R1A2C2010309, NRF-2020K1A4A7A02095438) and by the Brain Korea 21 Plus Program (Human Resource Center for Novel Materials Research Experts) (No. F19SR21D1101). S.K. was supported by the Samsung Research Funding Center of Samsung Electronics under project No. SRFC-IT1901-11.

## Author contributions

H.-W.L., J.-I.H., and S.K. designed and supervised this study. T.H.T.N. conducted all experiments. V.Q.N. and S.C. contributed to the epitaxial growth of films. S.J., E.P., H.J., and N.J.L. contributed the electrical measurements. S.L. and B.-G.P. contributed to the device fabrication. T.H.T.N., H.-W.L., J.-I.H., and S.K. wrote the paper.

## Competing interests

The authors declare no competing interests.

**Additional information**

**Supplementary information** The online version contains supplementary material available at <https://doi.org/10.1038/s42005-021-00743-9>.

**Correspondence** and requests for materials should be addressed to Hyun-Woo Lee, Jung-Il Hong or Sanghoon Kim.

**Peer review information** *Communications Physics* thanks the anonymous reviewers for their contribution to the peer review of this work. Peer reviewer reports are available.

**Reprints and permission information** is available at <http://www.nature.com/reprints>

**Publisher's note** Springer Nature remains neutral with regard to jurisdictional claims in published maps and institutional affiliations.



**Open Access** This article is licensed under a Creative Commons Attribution 4.0 International License, which permits use, sharing, adaptation, distribution and reproduction in any medium or format, as long as you give appropriate credit to the original author(s) and the source, provide a link to the Creative Commons license, and indicate if changes were made. The images or other third party material in this article are included in the article's Creative Commons license, unless indicated otherwise in a credit line to the material. If material is not included in the article's Creative Commons license and your intended use is not permitted by statutory regulation or exceeds the permitted use, you will need to obtain permission directly from the copyright holder. To view a copy of this license, visit <http://creativecommons.org/licenses/by/4.0/>.

© The Author(s) 2021